Nitrogen cycle dynamics during the Cretaceous Oceanic Anoxic Event 2 (OAE2; ~94 Ma) in the Western Interior Seaway

By

Jonn M van Oosten-Edl

Department of Geological Sciences, University of Colorado at Boulder

April 3rd, 2019

Thesis Advisor:

Julio Sepúlveda, Department of Geological Sciences

Defense Committee:

Julio Sepúlveda, Department of Geological Sciences

Brian Hynek, Department of Geological Sciences

Eve-Lyn Hinckley, Environmental Studies

Kathryn Snell, Department of Geological Sciences

Table of Contents

List of Figures

List of Tables

List of Appendices

Abstract:

The Cretaceous Ocean Anoxic Event 2 (OAE2, ~94 Ma), a time period of high sea-level and a warm greenhouse climate, was characterized by enhanced marine productivity and carbon burial in sediments, which resulted in the widespread deposition of black shales and a global perturbation of the carbon cycle. While decades of research have disentangled complex ecological dynamics during OAE2, a detailed understanding of the nitrogen cycle during this event (i.e., nitrogen transformations through metabolic and/or water-column redox reactions), remains elusive. I present a high-resolution (~300-3,000 years) bulk organic nitrogen stable isotope record from an expanded sedimentary section of OAE2 in the Smokey Hollow #1 core (SH1, southern Utah) that provides a record of changes in marine biogeochemistry from a marginal setting in the Western Interior Seaway (WIS). The $\delta^{13}C_{org}$ record shows the characteristic chemostratigraphic phases of OAE2 seen globally. The $\delta^{15}N_{org}$ record shows a 2-phased ^{15}N depletion of ~6‰, which is a larger than has been previously reported during OAE2, and may suggest a buildup of ^{15}N depleted ammonium from efficient nitrogen remineralization. Variations in the C/N ratio from 1.8 to 30.2 reflect variable input of organic matter sources to the study area throughout the event, including terrestrial (soil) and marine organic matter. The $\delta^{15}N_{org}$ record exhibits a moderate but statistically significant correlation with available data on terrestrial-derived biomarkers, likely reflecting the impact of transgressional sequences and/or terrestrial input on nitrogen cycle dynamics at this study location. My results indicate that nitrogen cycling in the western margin of the WIS was affected by increased recycling of ammonium in the oceans, as well as changes in nitrogen input from continental sources, across OAE2.

I. Introduction:

Oceanic Anoxic Events were time periods that generally lasted less than a million years when ocean basins experienced sustained or periodic reduction in oxygen levels, including anoxia and euxinia (the presence of free hydrogen sulfide) (Takashima et al., 2006). Oceanic Anoxic Event 2 (OAE2, ~94 Ma) was a time of maximum sea-level rise and peak temperatures over the past 100 million years (Fig. 1), characterized by enhanced marine productivity and carbon burial in sediments, which is reflected in a large and positive $\delta^{13}C$ excursion in carbonates and organic matter during OAE2 indicative of a global perturbation of the carbon cycle (Kuhnt et al., 2017; Jones et al., 2019). This led to the formation of organic-rich black shales under oxygen-poor conditions (e.g., black dots in Fig.2). Oxygen depletion appears to have been caused by unusually elevated primary productivity and a resulting increase in oxygen-consuming respiration (Kuypers et al., 2002; Meyer and Kump, 2008). The increase in productivity has been attributed to enhanced nutrient delivery from the emplacement and weathering of fresh oceanic and continental crust, large igneous provinces, seafloor spreading, and subduction zone volcanism (Fig. 2; Hays and Pitman, 1973; Kominz, 1984; Larson, 1991; Kerr, 2005; Flogel et al., 2011; Adams et al. 2010; Barclay et al., 20101; DuVivier et al., 2014; DuVivier et al., 2015).

OAE2 may have experienced sea surface temperatures as high as ~35ºC (O'Brien et al., 2017), which resulted from atmospheric CO_2 levels at least twice as high today (Hong and Lee, 2012). Thus, climate conditions during OAE2 were similar to what is anticipated for the foreseeable future on Earth under a "business as usual" scenario (Pachauri and Meyer, 2014), making OAE2 a useful case-study to interrogate climate feedbacks in the Earth system.

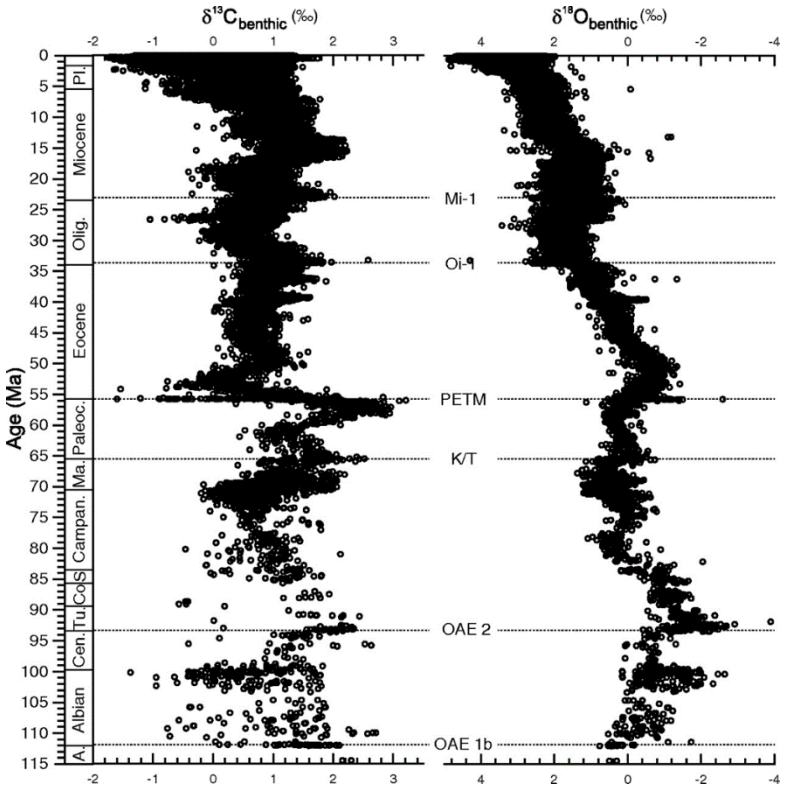

Figure 1: Carbon and oxygen isotope data from benthic foraminifera showing the perturbation of the carbon cycle, peak temperatures in ocean bottom waters during OAE2, and other boundary events during the past 115 Ma. More negative $\delta^{18}O$ values indicate warmer temperatures (Friedrich et al., 2012).

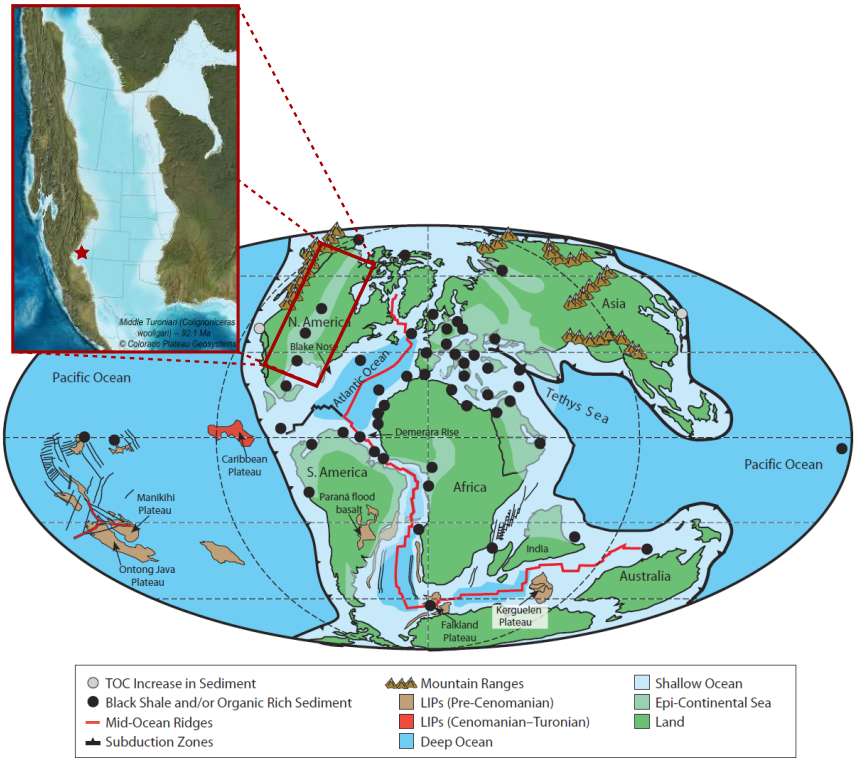

Figure 2: World map showing the position of continents and ocean basins during OAE2 the red box provides a close up of the WIS. (Takashima et al., 2006 *modified*). The red star indicates the location of SH1 in insert (Blakey and Ranney, 2018 *modified*).

While decades of research have disentangled some of the complex biogeochemical dynamics during OAE2, a detailed understanding of the nitrogen cycle during this event (i.e., nitrogen transformations through redox-controlled microbial processes), remains elusive. Previous work on nitrogen cycling during OAE2 has revealed some unique characteristics, including unusually high carbon to nitrogen ratios (C/N) and ^{15}N-depleted $\delta^{15}N_{org}$ values of bulk sedimentary organic matter (e.g., Rau et al., 1987; Junium and Arthur 2007). While these characteristics have been corroborated in a number of studies (e.g., Kuypers et al., 2004; Ohkouchi et al., 2006), interpretations of these signals are highly disputed. Additional records from different basins and depositional environments are still required to provide more robust interpretations. There is currently no consensus on the operation of the nitrogen cycle during OAE2, and factors such as rates of production/deposition, anoxia, and or water column circulation likely contribute to changes in nitrogen cycling. Some argue that the ^{15}N-depleted values seen during OAE2 indicate that nitrogen fixing organisms (diazotrophs) became the sole source of nitrogen in marine environments during this event (e.g., Kuypers et al., 2004). On the other hand, compound-specific work by Higgins et al. (2012) suggests an alternative interpretation of $\delta^{15}N_{org}$ trends during OAE2: low $\delta^{15}N_{org}$ values may represent the utilization of ^{15}N-depleted un-oxidized ammonium from oxygen-deficient waters by primary producers in surface waters (Higgins et al., 2012).

I present a high-temporal-resolution (centennial to millennial time scales) bulk elemental and stable isotope records of carbon and nitrogen from a rock core (Smokey Hollow #1; SH1) from the western margin of the Western Interior Seaway (WIS) that allows the study of nitrogen

cycling in shallow-water, near-shore environments during OAE2. The vast body of work available from the Smokey Hollow #1 (SH1) core (biomarkers, $\delta^{13}C_{org}$, and astrochronological dating) provides a comprehensive framework to assess the effects of variable marine productivity, terrestrial input, and water column deoxygenation on nitrogen cycling during OAE2. Given the high sedimentation rates of the SH1 core, my record helps to disentangle nitrogen cycling changes on timescales (~300-1000 years) that are relevant for our understanding of future potential scenarios of climate change during the Anthropocene.

II. Background:

Nitrogen is a critical element for life on Earth. However, the vast majority of nitrogen in the environment is present in the form of N_2 gas, which is not a usable form for organisms. To be useful for life nitrogen must be 'fixed' or changed into other nitrogen species such as nitrate (NO_3^-) or ammonium (NH_4^+) that are accessible for assimilation by primary producers. The nitrogen cycle incorporates the complex biological and abiotic processes that converts nitrogen into and out of various biologically useful forms. The Cretaceous OAE2 was characterized by abnormally high carbon to nitrogen ratios (C/N) and unusually ^{15}N-depleted $\delta^{15}N_{org}$ values of bulk organic matter (Table 1), which indicate a highly perturbed nitrogen cycle during this time. Disentangling the causes of these characteristics in the nitrogen cycle is a difficult process and still under much debate.

Location	pre-OAE2 $\delta^{15}N_{org}$	OAE2 $\delta^{15}N_{org}$ minimum	Shift	Reference
Central Open Ocean (Atlantic)	1.8	-1.1	-3	Baroni et al., 2015
	3.75	-0.66	-4.4	Rau et al., 1987
Southern Open Ocean (Atlantic)	-1.3	-1.4	-0.1	Kuypers et al., 2004
	5	2.3	-2.7	Rau et al., 1987
Southern Coast (Atlantic)	-0.9	-1.9	-1	Higgins et al., 2012 Junium and Arthur, 2007
	5.7	1.45	-4.25	Rau et al., 1987
North Coast (Atlantic)	1.4	1.3	-0.1	Baroni et al., 2015
North-Eastern Coast (Atlantic)	1.4	0.9	-0.5	Baroni et al., 2015 Blumenburg and Wiese, 2012
Western WIS	4	-2	-6	This study
Proto-Mediterranean	-0.7	-2.7	-2	Ohkouchi et al., 2006

Table 1. Summary of $\delta^{15}N$ signatures across OAE2. Data from Baroni et al., (2015), Ohkouchi et al., (2006), Rau et al., (1987), and this study.

II.a. Nitrogen Cycle systematics

The first step in the process of disentangling changes in the nitrogen cycle involves and understanding of the sources, transformations, and sinks of nitrogen in the environment (Fig. 3). The two major sources of nitrogen into the marine system are terrestrial input and marine nitrogen fixation. Terrestrial input is controlled by continental hydrology, which brings organic and inorganic nitrogen, along with other nutrients, into the system via weathering and runoff. Marine inputs come predominantly from diazotrophic (nitrogen-fixing) organisms. Nitrogen fixation is the conversion of inorganic nitrogen (N_2) into the usable ammonium form (Gruber and Sarimiento, 1997; Deutsch et al., 2007). After nitrogen has been fixed and brought into the system it can undergo various transformations. Ammonium can be oxidized to nitrate through a process called nitrification. Phytoplankton can assimilate nitrogen as either nitrate or ammonium

during photosynthesis, and respiration by heterotrophs releases nitrogen from biomass in the form of ammonium, which can then be assimilated by other organisms or oxidized to nitrate. Some of this nitrate can then also be assimilated or removed through denitrification, dissimilatory nitrate reduction to ammonium (DNRA), or anaerobic ammonium oxidation (anammox) in oxygen-depleted waters. The nitrate that escapes from denitrification processes, along with ammonium and other nutrients, can be returned to surface waters via upwelling to fuel productivity. Ultimately, nitrogen can also be removed by denitrification in sediments, or preserved in the form of ammonium adsorbed to clay minerals and organic matter.

II.b. Nitrogen isotopes as tracers of nitrogen cycling

Each of the processes controlling the speciation of nitrogen in the environment exhibit a different preference for ^{14}N over ^{15}N, called isotopic fractionation, which affects the $\delta^{15}N$ of nitrogen species pools being utilized and produced. The relative proportion of these two nitrogen isotopes in the environment is reflected in the delta notation as seen in equation one where,

$$\delta^{15}N(‰\ vs\ Air) = \left[\frac{\left(\frac{^{15}N}{^{14}N}\right)sample}{\left(\frac{^{15}N}{^{14}N}\right)air} - 1\right] \times 1000 \qquad (1)$$

and values are expressed in per mille (‰) vs air. In this notation the $\delta^{15}N$ of atmospheric N_2 is 0‰. Because each process ultimately affects the $\delta^{15}N_{org}$ of nitrogen preserved in sediments, measuring the $\delta^{15}N_{org}$ of sedimentary nitrogen can elucidate nitrogen cycling in the water column. The fractionation factors for most of these processes vary greatly (Fig. 3). For the inputs, fractionation factors (the isotopic offset between the reactant and product nitrogen chemospecies) for continental runoff and nitrogen fixation are in the ranges of -20 to +15‰, and 0 to -1‰, respectively (Popp, 2006). The wide range of values from terrestrial $\delta^{15}N_{org}$ reflects the multiple potential nitrogen sources in this environment, from soil-bound nitrogen to plant matter nitrogen, and the weathering of exposed sedimentary rocks. The values for nitrogen fixation derive from the slight preference for ^{14}N by the nitrogen fixing enzyme nitrogenase. Atmospheric deposition from anthropogenic processes such as fossil fuel combustion and nitrogen fertilizer use, on the other hand, can be anywhere from – 13‰ to + 2‰ in the modern (Popp, 2006). It is, however, difficult to assess the values and amount of natural atmospheric nitrogen deposition during the Cretaceous. For the outputs, microbial denitrification ranges from +20‰ to +30‰ in the water column, and ~0‰ in sediments (Popp, 2006). The isotopic fractionation associated with assimilation also varies greatly, whether it is of nitrate or ammonium, from +4‰ to +27‰ (Sigman et al., 2009). Due to the modern ocean's relative proportion of denitrification and fixation, nitrate and sedimentary nitrogen is characterized by $\delta^{15}N$ values around 5‰ (Fig. 3). During OAE2, however, $\delta^{15}N_{org}$ values are characteristically more negative. The question then becomes: what causes these negative shifts in $\delta^{15}N_{org}$?

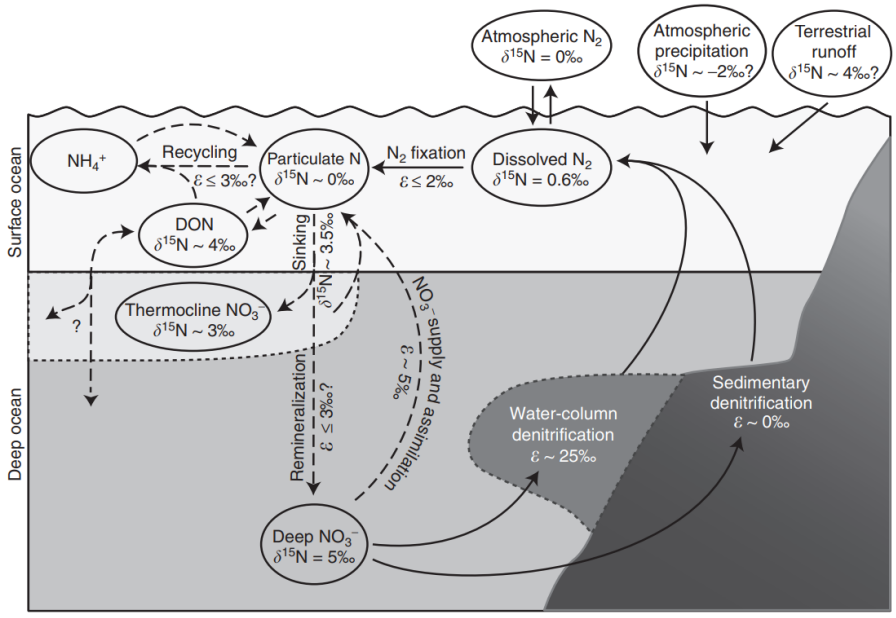

Figure 3: Illustration summarizing the different trends in $\delta^{15}N$ in the marine environment (Sigman et al., 2009). $\delta^{15}N_{org}$ values shown are averages of values available in 2009, hence the difference between values shown in figure and those mentioned in text.

II.c. Previous work on nitrogen cycling during OAE2

Two main hypotheses have been proposed to explain the depleted $\delta^{15}N_{org}$ values and high C/N ratios found in OAE sediments (Table 1; Fig. 4). The earliest interpretation of ^{15}N-depleted sedimentary nitrogen was that anoxic settings caused enhanced denitrification, leading to a deficit in marine nitrogen, ultimately allowing an increase of diazotrophy as the primary source of fixed nitrogen in the oceans (Fig. 4A; Rau et al., 1987; Kuypers et al., 2004; Junium and Arthur 2007; Kashiyama et al., 2008). Fixed nitrogen from diazotrophs produces, however, ^{15}N-depleted $\delta^{15}N_{org}$ values of only 0 to -1‰, which is problematic, since $\delta^{15}N_{org}$ values during OAE2 are typically much lower (Table 1). If diazotrophy were the sole cause of $\delta^{15}N_{org}$ depletion, then we would not expect the values to drop below – 1‰. Zhang et al. (2014) identified alternative nitrogenase enzymes that have the potential to produce more depleted $\delta^{15}N_{org}$ values on par with those reported from OAE2, but it is unlikely that those enzymes and associated organisms

were present at globally-significant abundances to produce the observed values, given their rare occurrence and minimal contribution in modern environments.

Higgins et al. (2012) used bulk and compound-specific measurements of nitrogen isotopes in porphyrins, the degradation products of chlorophyll, and constructed a mixing model that showed a distinct lack of diazotrophy during OAE2, challenging the original interpretations. Instead, these authors proposed a nitrogen cycle with enhanced remineralization to explain the ^{15}N-depleted $\delta^{15}N_{org}$ values. Remineralization under the right circumstances (low nitrification rates) can yield ^{15}N-depleted ammonium (the fractionation factor for ammonium assimilation is greater than that of nitrification when there is more ammonium than nitrate). This remineralized ammonium would then be reused in the nitrogen cycle again and again, becoming progressively ^{15}N-depleted and eventually reaching levels that would equal the depleted values seen in previous records (Fig. 4B).

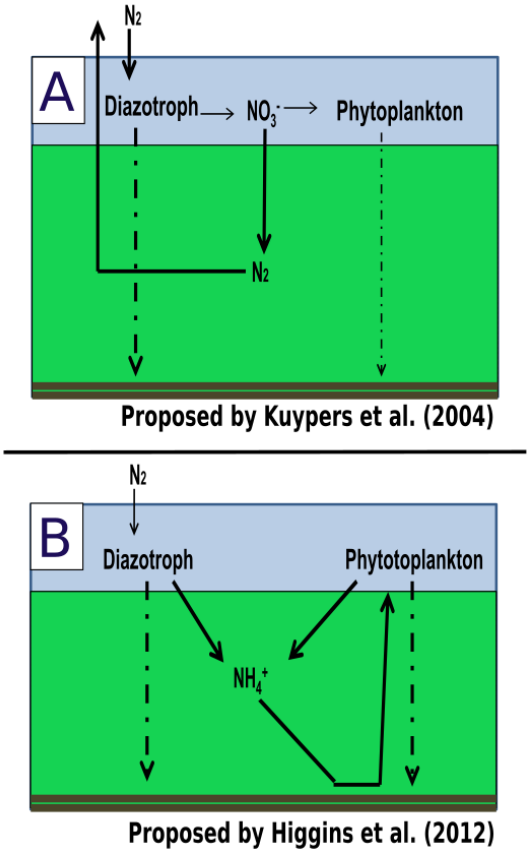

Figure 4: Simplified graphical representation of the hypotheses described to explain nitrogen cycling during OAE2 by (A) Rau et al., (1987); Kuypers et al., (2004); Junium and Arthur (2007); Kashiyama et al., (2008); and (B) Higgins et al. (2012).

II.d. Scope of work

The majority of nitrogen isotope records during OAE2 derive from sediment cores from the North Atlantic, where low sedimentation rates lead to low-temporal resolution studies. The low temporal resolution and bias to one basin makes it difficult to understand the finer dynamics of nitrogen cycling during OAE2, particularly in more coastal settings. Also, these records rely on $\delta^{15}N_{org}$ to infer deoxygenation but have few (if any) independent means to constrain deoxygenation in relation to nitrogen cycling.

I present a high-resolution stable isotope record from an area with high sedimentation rates that sheds new light on the complex dynamics of nitrogen cycling at play during OAE2, especially when interpreted along with existing lipid biomarker data. *I tested the hypothesis that changes in nitrogen cycling in a nearshore environment of the WIS were more dynamic than open ocean sites, and were influenced by the combined effects of water column oxygenation and terrestrial input.*

III. Methods:

87 black shale samples from the SH1 core, collected in 2014 near Grand Staircase – Escalante National Monument (Fig. 5), were analyzed for bulk elemental and stable isotope total nitrogen and organic carbon geochemistry using an Elemental Analyzer-Isotope Ratio Mass Spectrometer (EA-IRMS) in the CU Boulder Earth Systems Stable Isotope Lab.

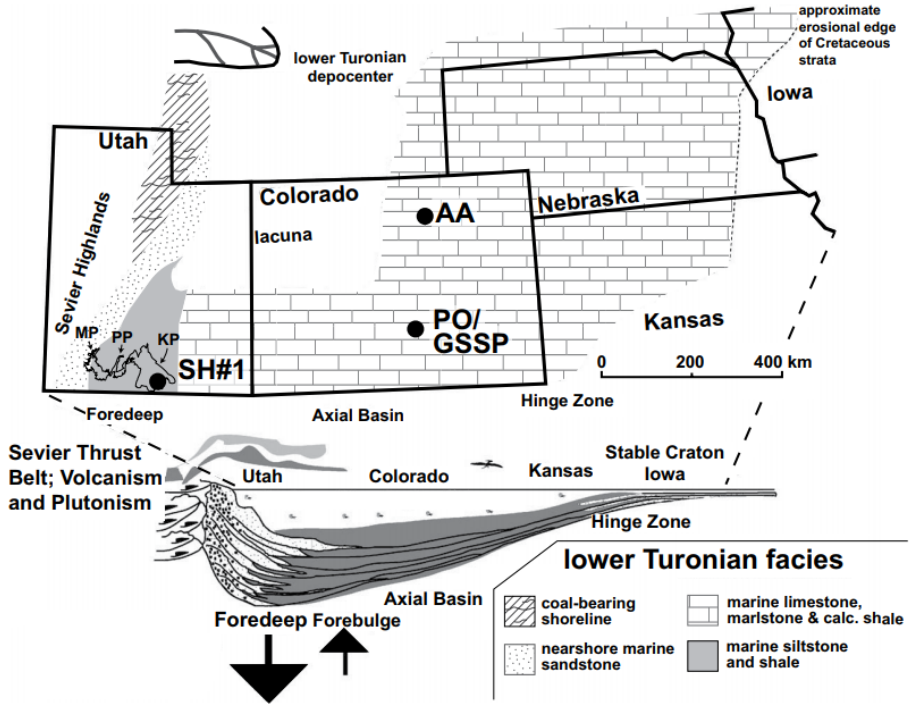

Figure 5: Location of the SH1 core in southern Utah. Cross section (below) shows local subsidence of depositional environment, map view (above) shows geographic location of the SH1 core (Jones et al., 2019).

The SH1 core was recovered from Big Water, Utah in the summer of 2014. The entire core is 131.15 meters long and is characterized by lithological changes that vary mostly between calcareous shale and marl, with some layers of sandstone and mudstone near the start of the core, and bentonite beds scattered throughout. The SH1 core contains a complete, expanded (~30 meters) record of OAE2. Jones et al. (2019) provides a detailed description of the lithology, cyclostratigraphy, and astrochronology of the SH1 core. The high-resolution portion of my data set begins at a depth of 123.00 meters core depth (mcd) and ends at 115.00 mcd. Sampling resolution during this interval reflects roughly 300 years of time between each sample. The rest of the core was studied at lower temporal resolution, with samples collected every 1–2 m, representing roughly 3,000 years of sedimentation between samples. For all samples, 2 mm of the outer rock was removed using a Dremel wire brush and a metal spatula. Samples were then crushed using a mortar and pestle. The powdered rock samples used in this study were previously extracted for lipid biomarkers using a Dionex Accelerated Solvent Extractor with dichloromethylene: methanol 9:1 (v:v). Before EA-IRMS analysis, samples were decalcified as

explained below. I tested several sample preparations and analytical methods to optimize analytical accuracy and sample throughput, the results of which can be found in Appendix 1. I used five standards (L. Glutamine, acetanilide #1, Pugel, B2153 - Known Organic Soil, B2152 - Low Organic Soil) to assess carbon and nitrogen percent as well as $\delta^{13}C_{org}$ and $\delta^{15}N_{org}$ throughout this study.

III.a. Decalcification of samples

Carbonate was removed in all 87 samples using 10% Hydrochloric acid following the CUBES lab procedure, which is an adaptation of the method outlined by Brodie et al. (2011). This allowed me to determine the percent carbonate per sample and accurately measure the $\delta^{13}C_{org}$, percent of total organic carbon (TOC%), percent of total organic nitrogen (TON%), and establish carbon/nitrogen (C/N) ratios. Three grams of each sample were weighed out and placed into glass centrifuge tubes. 10 mL of 10% HCl was then added to each sample, vortexed, and allowed to fully react. The samples were then centrifuged at 1000rpm for 3 min. Roughly, 85% of the acid solution was pumped out, leaving ~15% to reduce sample loss. Milli-Q water was then added to each sample and vortexed. The samples were then centrifuged and the liquid was again pumped off. This process was repeated until the pH of the solution matched that of the Milli-Q water. At this point, the remaining water was pumped off and the samples were then dried in an incubation oven at ~26° C for ~3 days, or until fully dry. The samples were then crushed again to ensure homogeneity and weighed to determine $CaCO_3$%. Results can be found in Appendix 2.

IV. Results:

IV.a. TOC%, TON%, and C/N

TOC% ranged between 2.7% and 0.08% (Fig. 6). The record began with a large drop from 2.7% to 0.48% at 124.6 mcd. The record then showed a step-wise increase to 1.8% at 122.5 mcd. TOC% then dropped to 0.17% at 122.3 mcd and spiked again to 1.3% at the start of OAE2. After this spike values for TOC% reached their lowest point 120.1 mcd and stayed consistently low from 120.7 to 118.1 mcd. The record then showed a generally increasing trend from 117.7 to 107.9 mcd. At 105.1 mcd TOC% dropped 0.4% and then rose to 1.2% at 102.9 mcd (the end of OAE2). After this point the values remained fairly consistent (around 1.2%) until the end of the record at 94.6 mcd, with the exception of a small dip at 96.9 mcd. TON% ranged between 0.09 % and 0.02%. The record of TON% (Fig. 6) showed much more variability than the TOC%, but it appeared to share the same trends from 122.7 mcd to 119.85 mcd. The differences in the x-axis on TOC% and TON% should be noted as TON% never rose above 1% while TOC% ranged from 0.08% to 2.7%, suggesting that the C/N ratio in this record was more sensitive to carbon than nitrogen.

The notable exception to this pattern can be seen at 111.8 mcd, where a steep drop in TON% contributes to the spike in the C/N ratio. The C/N ratio (Fig. 6) ranged between 1.8 and 30.2 and showed a large decrease from 30.23 to 9.71 at the base of the core before the positive CIE between 121.295 and 102.89 mcd, followed by a spike just prior to the onset of OAE2. The C/N ratios exhibited the lowest values between 120.45 and 115.89 mcd and high variability between 125.15 and 102.89 mcd. After OAE2, C/N values show more stable and intermediate values. Standard deviations can be found in the meta data file included in the Appendix. The gap from 107.9 mcd to 105.1 mcd is due to the unusable values obtained from a sample at 106.9 mcd. Due to problematic values from multiple runs further work is needed to properly analyze these samples.

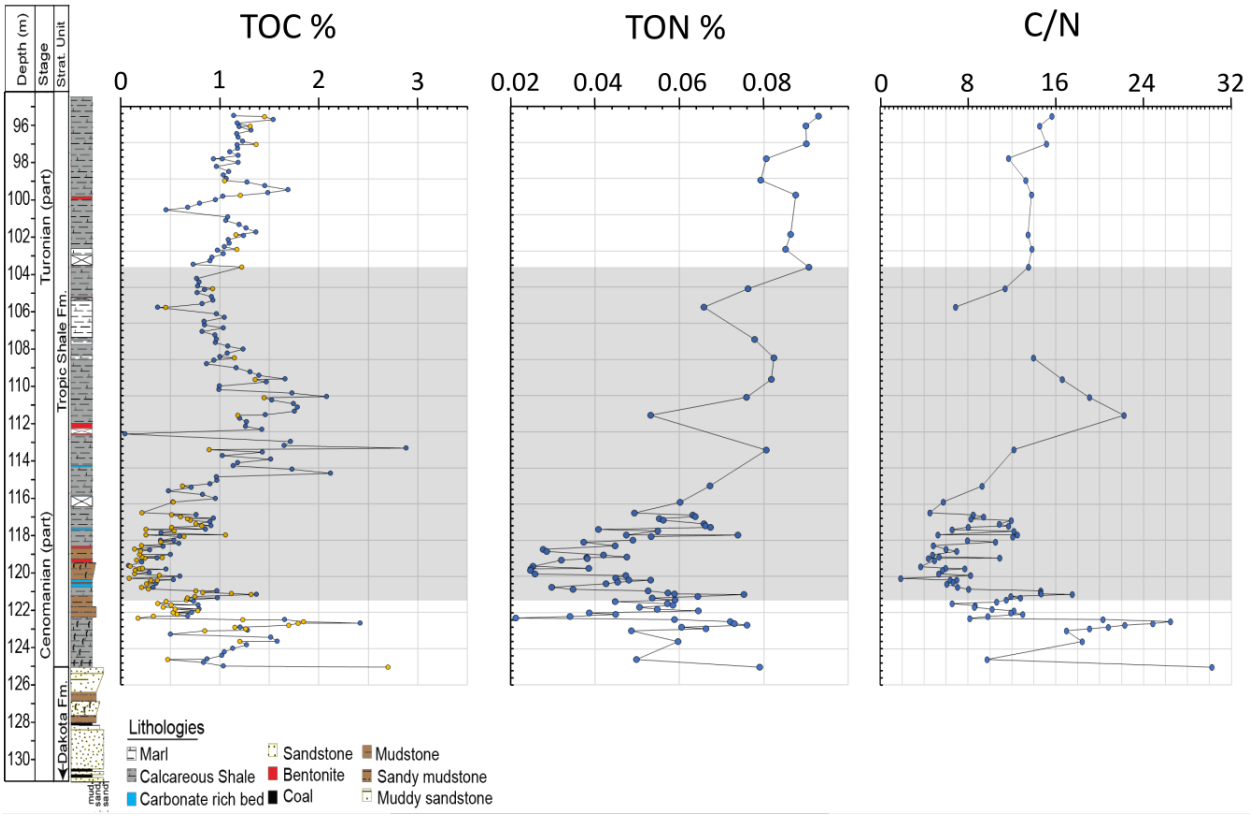

Figure 6: TOC%, TON%, and C/N ratio vs Depth in meters. The gray shaded region indicates the OAE2 interval. The TOC% dataset contains data from Jones et al., (2019; blue symbols) and from this study (orange symbols).

IV.b $\delta^{13}C_{org}$

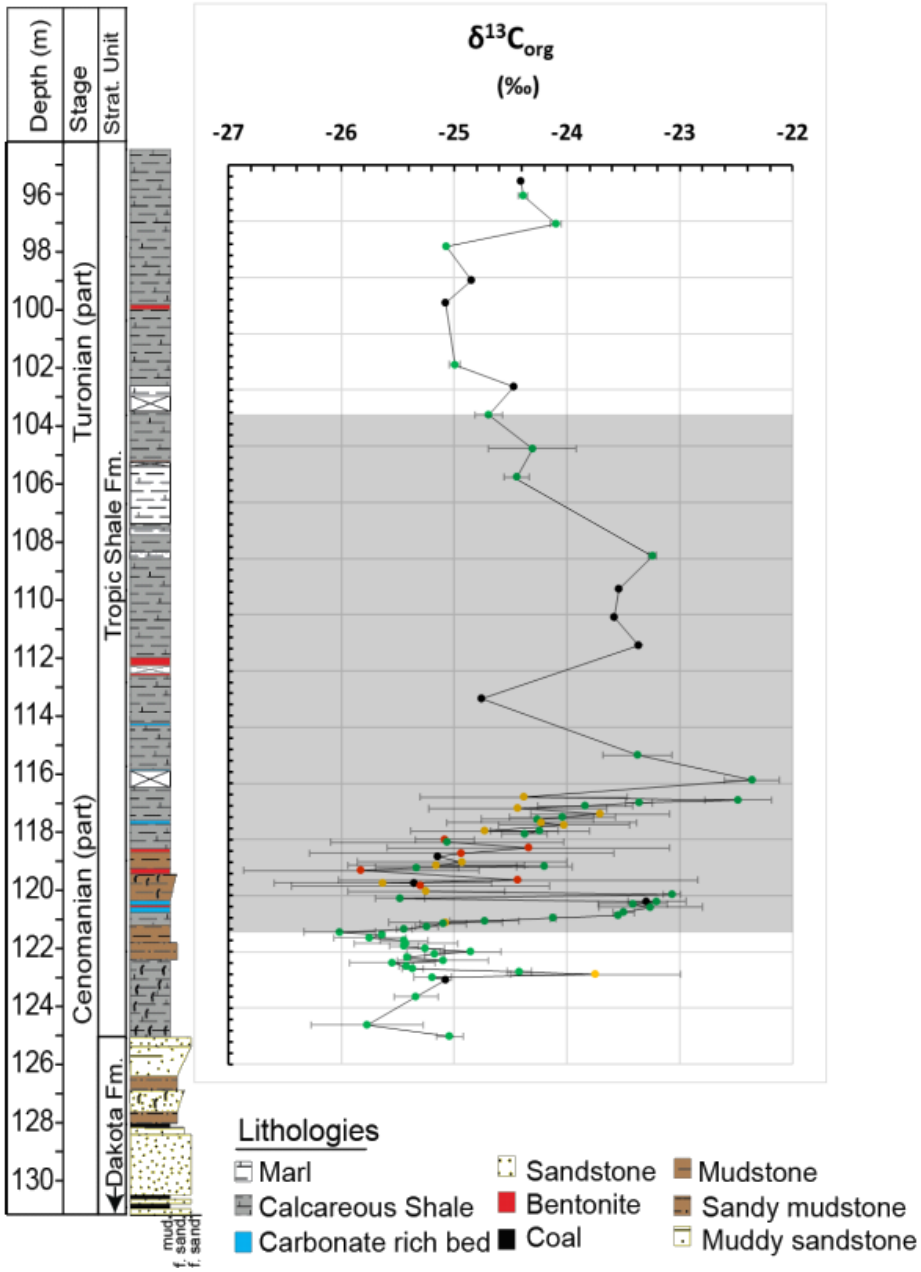

Figure 7: $\delta^{13}C_{org}$ vs Depth. Green points represent samples with standard deviation values ranging from 0 – 0.5‰. Yellow points represent samples with standard deviation values ranging from 0.5 – 1.0‰. Red points represent samples with standard deviation values > 1.0. Black points represent samples which were only run once. OAE2 interval is indicated by the gray shaded region. The stratigraphic column is adapted from Jones et al., (2019).

Bulk organic carbon isotopes ranged between -22.3‰ and -26.02‰ (Fig. 7). During the interval 125.015-121.295 mcd (pre-OAE2), values ranged between -25.03‰ and -26.01‰, with a large positive spike of 1.29‰ at 122.805 mcd. OAE2 begins at 121.295 mcd with a large positive shift in $\delta^{13}C_{org}$ of 2.94‰, followed by a decrease down to -25.82‰ at 119.1 mcd. The section from the onset of OAE2 until 115.89 mcd showed a high degree of variability, but also a generally positive trend that peaks at -22.36‰ at 115.89 mcd. After this point values drop down to -24.76‰ at 113 mcd and then experience a quick rise back up to -23.36‰ at 111.08 mcd. The

values appear to remain more consistent after this point for the next three samples. The gap at 106.9 mcd is due to the previously explained absence of a sample at 106.9 mcd.

OAE2 ends at 102.89 mcd, where $\delta^{13}C_{org}$ values stabilize after this point, though they are still more elevated than the pre-OAE2 values. These results are consistent with a previously completed $\delta^{13}C_{org}$ record on the SH1 core during the same interval. I have compiled both records into Figure 8 and the combined ultra-high-resolution record shows highly dynamic environment during the onset of OAE2. The standard deviation for $\delta^{13}C_{org}$ values ranged from 0.01 – 1.59‰, with only six of the total number of samples having standard deviations above 1.0‰.

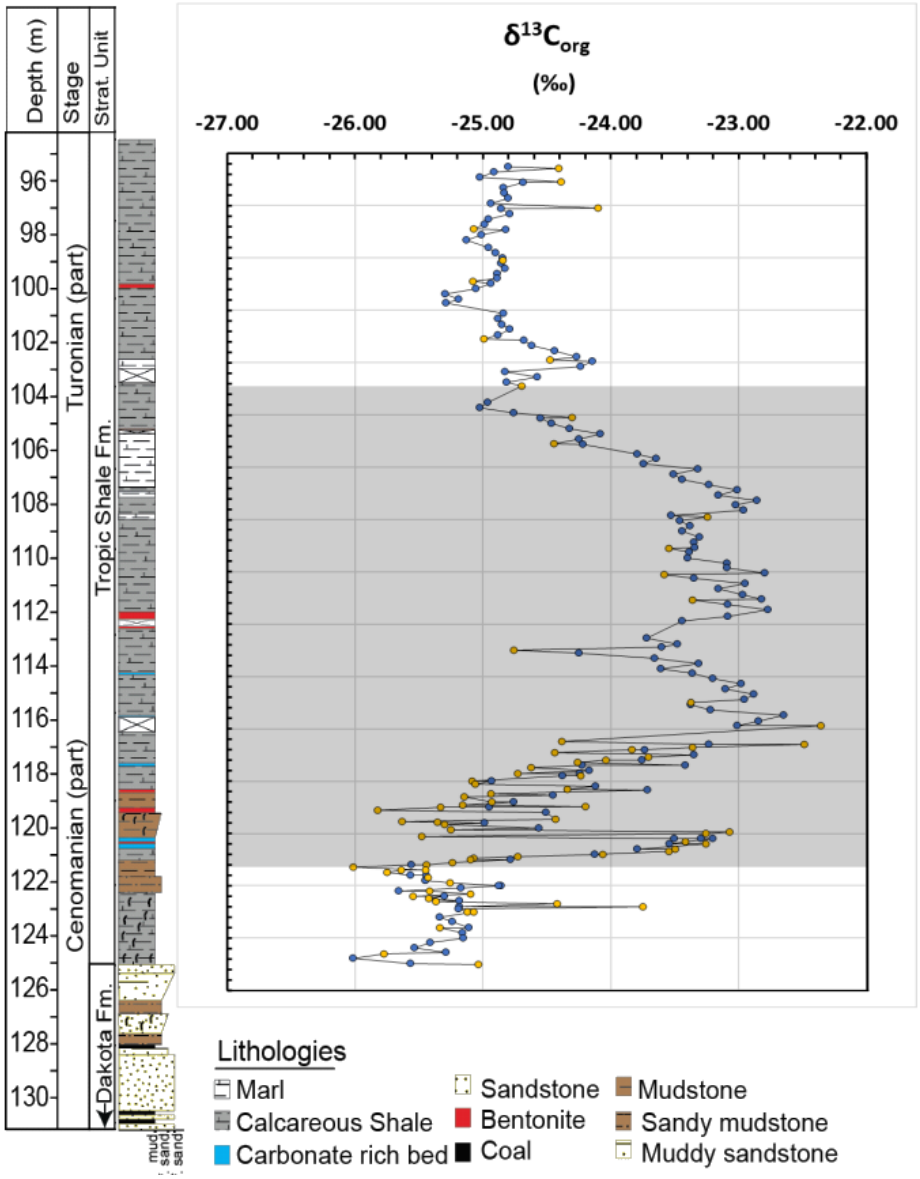

Figure 8: $\delta^{13}C_{org}$ vs Depth. A combined record of $\delta^{13}C_{org}$ values from this study (orange points) and $\delta^{13}C_{org}$ values from Jones et al., (2019) (blue points). The stratigraphic column is adapted from Jones et al., (2019). OAE2 interval is indicated by the gray shaded region.

IV.c $\delta^{15}N_{org}$

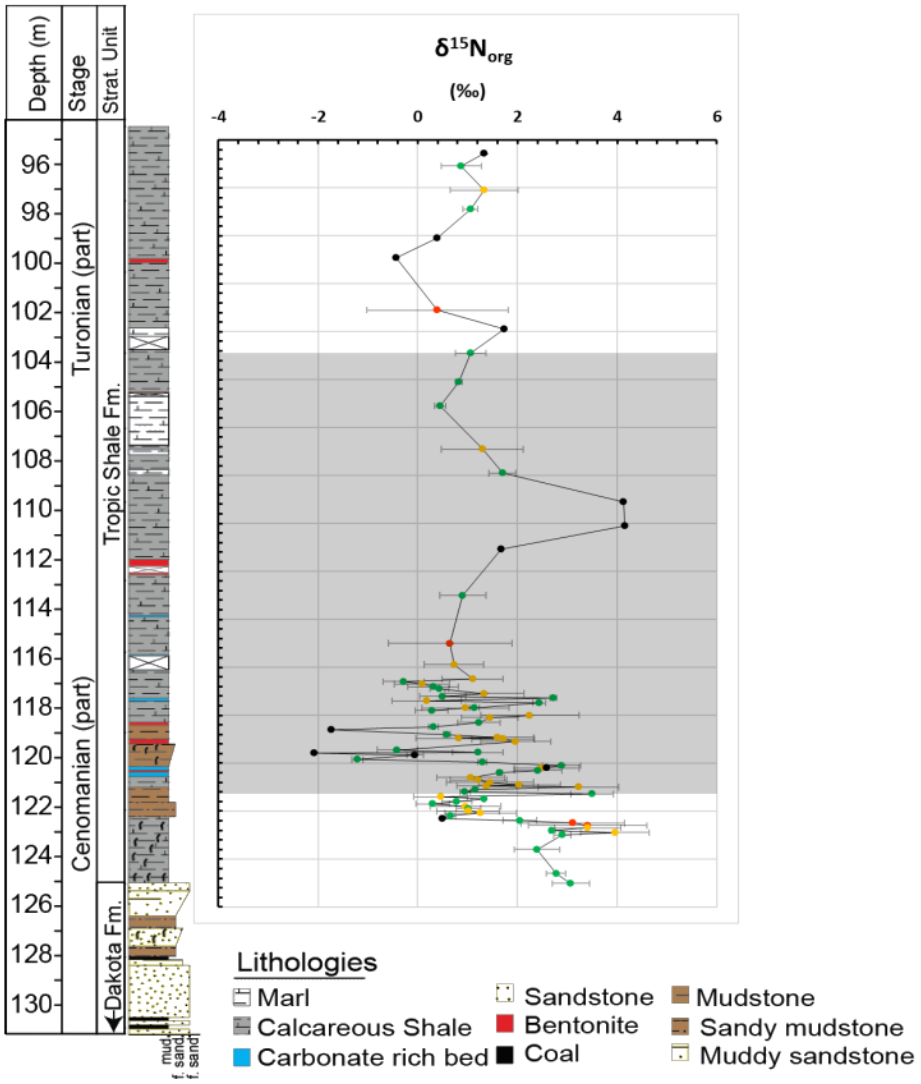

Figure 9: $\delta^{15}N_{org}$ vs Depth. Green points represent samples with standard deviation values ranging from 0 – 0.5‰. Yellow points represent samples with standard deviation values ranging from 0.5 – 1.0‰. Red points represent samples with standard deviation values > 1.0. Black points represent samples which were only run once. The gray region represents the time period of OAE2. The stratigraphic column is adapted from Jones et al., (2019).

$\delta^{15}N_{org}$ values ranged between 4.2‰ and -2.1‰ (Fig. 9). Prior to OAE2, $\delta^{15}N_{org}$ values between 125.015 mcd and 122.7 mcd are more positive, ranging from 2.39‰ to 3.96‰, with a small spike at 122.9 mcd. After 122.7 mcd, samples showed highly variable values with drastic positive and negative shifts in $\delta^{15}N_{org}$ of ~5‰. While the system was highly variable through the high-resolution portion of our data (123 – 116.46 mcd), there was a clear overall negative shift in $\delta^{15}N_{org}$. Between 116.49 mcd and 113 mcd $\delta^{15}N_{org}$, values appear to temporarily stabilize, but quickly make a drastic positive shift upwards to 4.15‰ at 110.1 mcd. This was followed by a quick shift back down to 0.45‰ at 105.1 mcd. The record appeared to be more stable after this point, but this may simply be due to the lower sampling resolution at this time. There was a smaller positive peak at 101.9 mcd just after the end of OAE2, and a valley at 98.9 mcd, but the

average of these last 11 points was 0.82‰, which was still much more negative than the pre-OAE2 starting values. The standard deviation for $\delta^{15}N_{org}$ values ranged from 0.0004 to 1.4‰, with only three of the total number of samples having standard deviations above 1.0‰.

V. Discussion:

V.a. Carbon and Nitrogen dynamics in SH1

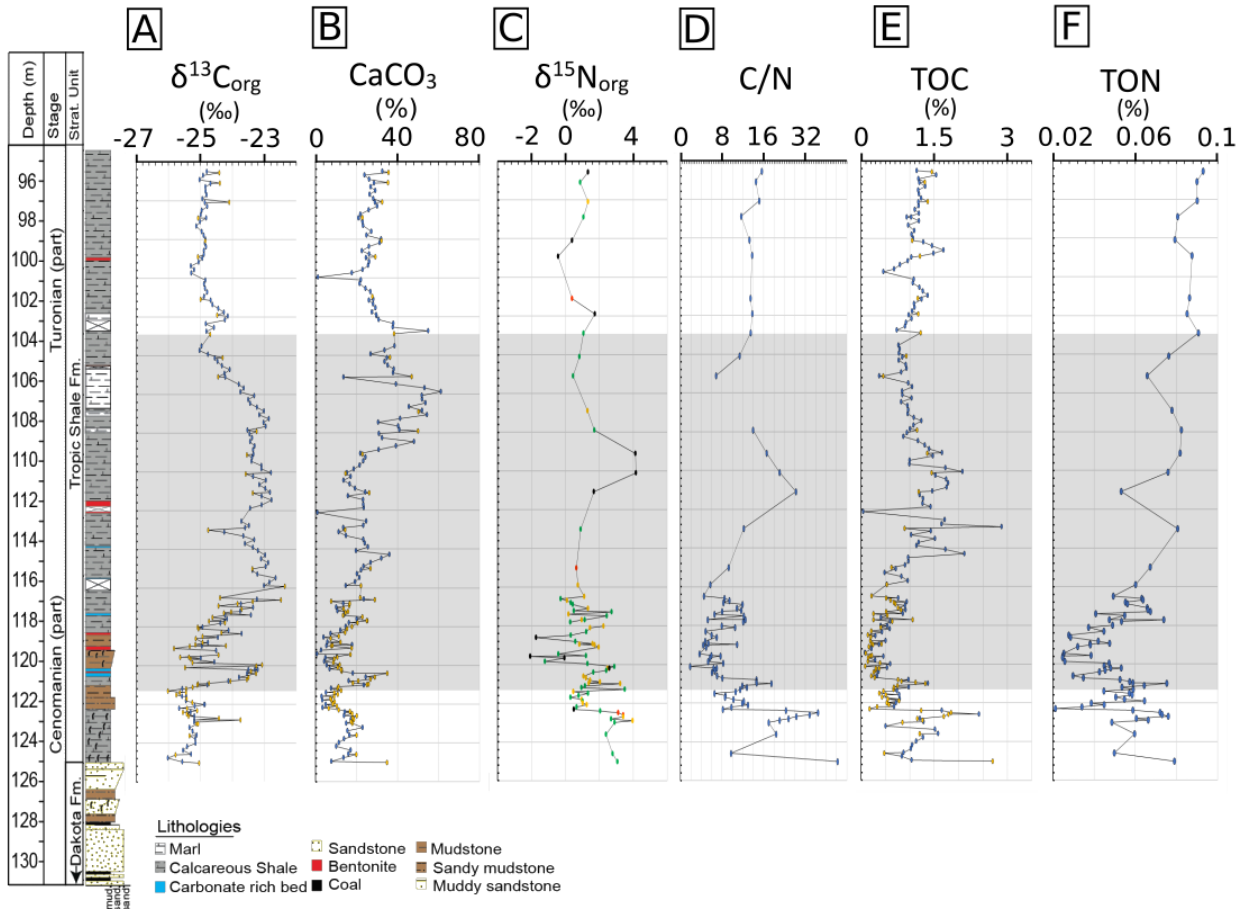

Figure 10: Elemental and stable isotope data from the SH1 core. The stratigraphic column is adapted from Jones et al. (2019). (A) Combined $\delta^{13}C_{org}$ record with data from Jones et al. (2019; blue symbols) and this study (orange symbols); (B) combined $CaCO_3$% record with data from Jones et al. (2019; blue symbols) and this study (orange symbols); (C) $\delta^{15}N_{org}$; (D) C/N ratio; (E) combined TOC% record with data from Jones et al. (2019; blue symbols) and this study (orange symbols); (F) TON%. OAE2 interval is indicated by the gray shaded region.

My record of OAE2 showed a dynamic system that appears to be primarily influenced by the mixing of terrestrial and marine end members, with the ^{15}N enriched nitrogen deriving from terrestrial sources and ^{15}N depleted nitrogen from marine sources, where marine nitrogen becomes ^{15}N depleted due to the effective remineralization and utilization of ammonium. We see this point reflected best in the records of $\delta^{15}N_{org}$ and the C/N ratio, which showed a moderate

but statistically significant correlation (see below). Decreases in $\delta^{15}N_{org}$ and C/N reflect a higher input of the marine nitrogen isotopic end-member, whereas increases in $\delta^{15}N_{org}$ and C/N reflect higher input from the terrestrial end-member. Both C/N ratios and $\delta^{15}N_{org}$ values are at their highest levels pre-OAE2 (below 122 mcd), likely reflecting enhanced continental input of nitrogen and organic matter (Fig. 10). Similarly, there was a spike in both the C/N and $\delta^{15}N_{org}$ at ~111 mcd, likewise reflecting a large influx of terrestrial nutrients into the system. Terrestrial nitrogen would have higher $\delta^{15}N_{org}$ values if the nitrogen is derived from wet soils that have been subject to significant denitrification, which would leave the remaining soil-bound nitrogen ^{15}N enriched. These increases in C/N and $\delta^{15}N_{org}$ occur during previously documented transgressions in sea-level at the time (Jones et al., 2019), supporting the hypothesis that these were intervals of enhanced terrestrial organic matter input to the SH1 core location.

Towards the onset of OAE2 at 121.295, $\delta^{15}N_{org}$ and C/N display a general downward trend until the peak of the $\delta^{13}C_{org}$ record at 115.89 mcd. This is best explained by increased influence (input) of marine nitrogen, where the water column has been affected by deoxygenation and ammonium build-up, driving down $\delta^{15}N_{org}$ values (Fig. 4A; Higgins et al., 2012).

At 116.49 mcd, the downward trend in $\delta^{15}N_{org}$ reversed, increasing back to pre-OAE2 values. This was also reflected in the C/N ratio, though the C/N peak occurs slightly before the $\delta^{15}N_{org}$ peak. The two are still likely tied together here, and this event likely reflects another large influx of terrestrial matter into the WIS, possibly caused by another sea-level transgression (Jones et al., 2019). An increase in continental runoff would provide nutrients to fuel enhanced productivity, leading to oxygen depletion (Peterson et al., 2016; Behrooz et al., 2018). However, we don't see low $\delta^{15}N_{org}$ values at this point, but actually the opposite, supporting an increased influence in ^{15}N enriched terrestrial nitrogen. While this is a time of higher sea level at the SH1 core location, the signal in $\delta^{15}N_{org}$ from the marine end member is being overprinted by an increased delivery of highly ^{15}N enriched terrestrial signal, which could be expected in a coastal environment. The reduction in TON% values is likely enhancing the C/N ratio in this interval. This dip in TON% might reflect an increase in terrestrial input as well, given the elevated C/N ratios of terrestrial organic matter compared with low C/N ratios of marine organic matter.

After the positive peak in $\delta^{15}N_{org}$ at 107.9 mcd, the values of $\delta^{15}N_{org}$, $\delta^{13}C_{org}$, and C/N stabilize and show much less variability until the end of the record. It should be noted that the C/N values still remain elevated compared to typical modern values and that $\delta^{15}N_{org}$ remains depleted compared to modern values; this is expected for marine systems during OAE2 (Rau et al., 1987). The smaller changes in C/N ratios towards the end of the record may be driven by changes in marine carbon export (i.e., changes in productivity).

In two instances the overall change in $\delta^{15}N_{org}$ was as large as -4.58‰ and -6.03‰. Both of these changes are larger than what has previously been reported in other records worldwide

(Table 1), and could be explained by the coastal, shallow water setting of the SH1 core. For instance, the starting $\delta^{15}N_{org}$ values at the base of the record were higher than many sites before the OAE2 event, which likely reflects an enhanced contribution of terrestrial input into the system. The addition of terrestrial matter raised the values of $\delta^{15}N_{org}$ and C/N by bringing in ^{15}N enriched nitrogen from the denitrification that takes place in soils and an increased amount of carbon from all of the soils organic matter (soil organic matter is generally higher than marine due to lignins from terrestrial plants). This raised the starting point of the $\delta^{15}N_{org}$ and C/N ratio values in my record (pre-OAE2, 125 mcd) and provided the necessary nutrients required for primary producers to substantially increase their activity, which then led to the deoxygenation of the marine environment. This deoxygenation was caused by enhanced respiration and remineralization, which converts organic matter to ammonium, and would have caused a decrease in nitrification, which uses oxygen to convert ammonium to nitrate. Phytoplankton then assimilated this ^{15}N depleted ammonium and when these phytoplankton died their organic matter was again remineralized causing the nitrogen contained within to become further depleted in ^{15}N, thus driving down $\delta^{15}N_{org}$ to values typical of OAE2. The higher starting point at this location thus contributed to a larger shift overall in the record of $\delta^{15}N_{org}$. The presences of two large shifts in $\delta^{15}N_{org}$ demonstrated the more dynamic nature of this site as these two large positive peaks in $\delta^{15}N_{org}$ demonstrated at least two large influxes of terrestrial matter into the site. The negative signal produced by the marine nitrogen isotopic end-member was likely overprinted by the higher positive terrestrial end-member during these elevated $\delta^{15}N_{org}$ value intervals. At the SH1 core location, the addition of terrestrially-derived nutrients into a marine system may have been a crucial component for explaining changes in productivity during OAE2.

V.b Comparison with existing biomarker data

Ongoing lipid biomarker work by CU graduate student Garrett Boudinot (Boudinot et al., *in prep*) allowed me to compare trends in the elemental and stable isotope composition of the SH1 core with changes in environmental conditions and marine productivity (Fig. 11). The oleanane index, the ratio of C_{28} steranes/all steranes, and 2-methylhopanes index showed significant correlations with my records (Figs. 11; Table 2).

The oleanane index, a biomarker derived from angiosperms used as an indicator of terrestrial input (Peters et al., 2005), positively correlates with $\delta^{15}N_{org}$ and the C/N ratio (Fig. 11A-C; Table 2). Pre-OAE2, values of the oleanane index are at their highest points in the record, similarly to those of the C/N ratio and $\delta^{15}N_{org}$, reflecting a larger terrestrial input into the system. At the onset of OAE2 (121.295 mcd), a steep drop across all three records likely reflects decreased terrestrial input and a relatively larger influence of marine end-member values. The high point in the oleanane index at 122.8 mcd corresponds with the previously mentioned transgression at the time. Additionally, similar peaks in all three parameters at ~110 mcd suggests the occurrence

of another large influx of terrestrial nutrients and organic matter. The peak in the oleanane index at ~105 mcd is not seen in the C/N ratio and $\delta^{15}N_{org}$, but in this case this may be due to the lower sampling resolution of my records in this interval. Also, because bulk organic records are controlled by many factors, it is not unusual to find differences between these and source-specific biomarkers records.

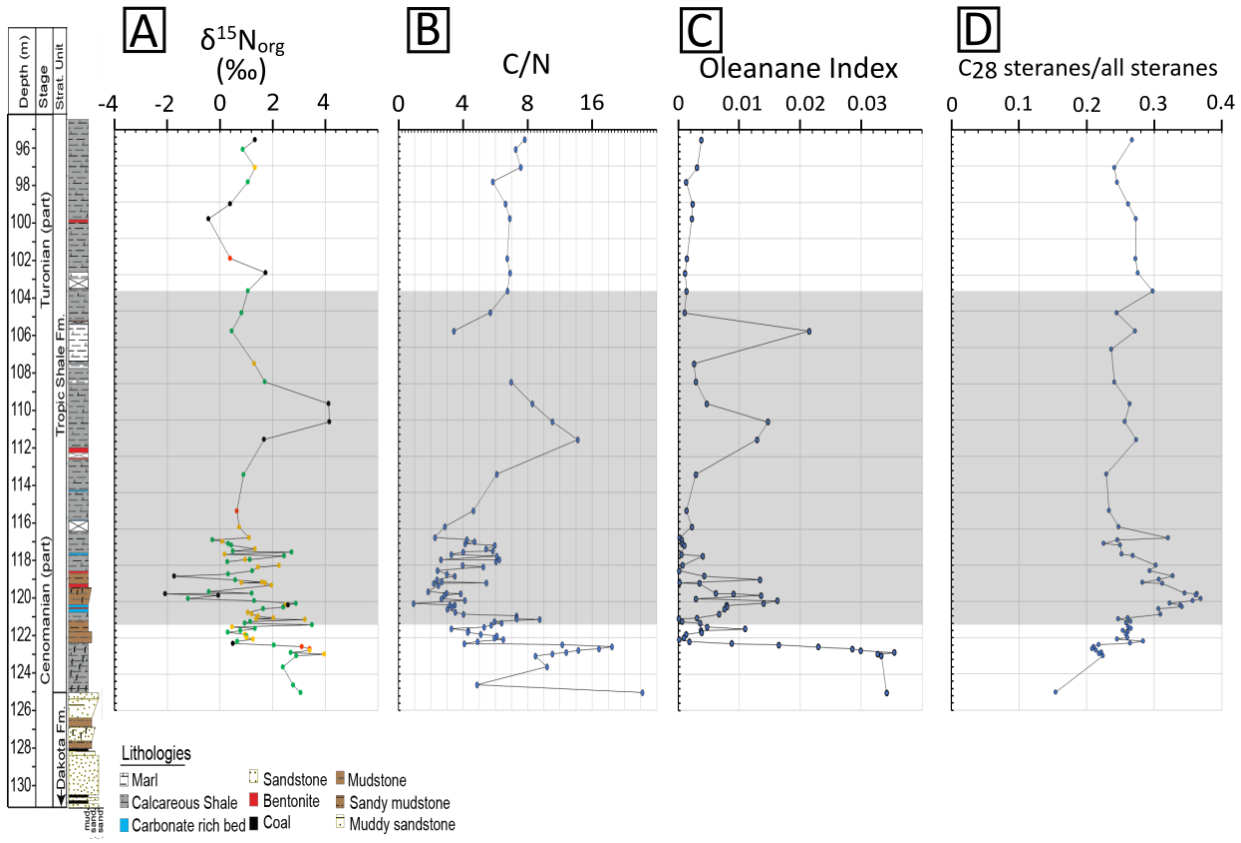

Figure 11: (A) $\delta^{15}N_{org}$, (B) the C/N ratio, (C) the Oleanane Index, (D) C_{28} steranes/all steranes. OAE2 interval is indicated by the gray shaded region.

The ratio of C_{28} steranes/all steranes and 2-methylhopane index also showed correlation with the C/N ratio (Fig. 11A, B, D; Table 2). The ratio of C_{28} steranes/all steranes reflects the relative proportion of prasinophyte algae over other algae. Prasinophyte algae prefer ammonium and so may be indicative of higher amounts of ammonium build-up in the system (Prauss, 2007). The comparison between C_{28} steranes and C/N indicates an inverse relationship (Table 2), which is demonstrated clearly in the peak in C_{28} steranes and the valley in C/N around 120 mcd (Fig. 11B, 11D). Following the description of events explained above, this could be attributed to increase deoxygenation, which also supports the model of increased ammonium build-up from Higgins et al. (2012).

Somewhat surprisingly, the carotenoid isorenieretane did not show statistically significant correlation with either C/N ratios or $\delta^{15}N_{org}$ (Table 2). This biomarker indicates the presence of

Chlorobi, a bacteria that requires hydrogen sulfide and sunlight, and thus indicate the presence of photic zone euxinia (Sinninghe Damsté and Schouten, 2006). This suggests that local deoxygenation, or at least photic zone euxinia, does not directly correlate with $\delta^{15}N_{org}$ or the C/N ratio as it has been assumed by others in the past. It should be noted that while the build-up of ammonium and upwelling are basin-scale processes, photic zone euxinia is likely a more localized phenomenon (Boudinot et al. *in press*), meaning that the lack of correlation here does not indicate a lack of anoxia. More work is needed to adequately determine the correlations between redox sensitive biomarkers, trace metals, and $\delta^{15}N_{org}$, to elucidate a more specific relationship with deoxygenation and nitrogen cycling.

In most cases, C/N and $\delta^{15}N_{org}$ show only moderate correlation with biomarker data (Table 2). This is not unusual if we consider that bulk geochemical data can be affected by multiple factors, including terrestrial input, marine productivity, water column deoxygenation, respiration in sediments, and diagenesis.

While the dominant trends in C/N and $\delta^{15}N_{org}$ in the SH1 core can be explained by changes in terrestrial input and deoxygenation, many questions remain and warrant further investigation. First, the decrease in $\delta^{15}N_{org}$ between 101.9 and 96.89 mcd in the post-OAE phase does not match with the previously discussed changes in the C/N ratio, or with any of the biomarker data. This suggests that other processes, likely marine nitrogen cycle changes, may have controlled the signals in this interval. Second, it appears that the $\delta^{15}N_{org}$ record might be driven by some cyclicity. While identifying cyclicity in these records is beyond the scope of this study, it is supported by the identification of orbitally-tuned cyclicity reported in the carbonate and $\delta^{13}C_{org}$ records of bulk organic and carbonate reported by Jones et al. (2019). Future work should assess the temporal periodicity of these cycles to identify if they are driven by changes in orbital cyclicity. Finally, comparison with more redox-sensitive biomarkers and trace metals would further help to disentangle the effect of local and regional deoxygenation on nitrogen cycling at the SH1 location.

Linear Regression	R^2	Slope	P - value
C/N ratio vs oleanane index	**0.312**	**0.0009**	**3.5223E-06**
$\delta^{15}N$ vs oleanane index	**0.2948**	**0.0042**	**6.164E-06**
C:N ratio vs 2MHI_100	**0.2982**	**0.0743**	**6.3807E-06**
C/N vs C28/allSt	**0.51**	**-0.005**	**1.4889E-10**
C/N vs $\delta^{15}N$	**0.2470767**	**2.25**	**2.3547E-06**
C/N vs Isorenieretane	**0.02419363**	**0.0834**	**0.20879691**
$\delta^{15}N$ vs Isorenieretane	**0.004**	**0.1516**	**0.60938878**

Table 2: Linear regressions. The C/N ratio vs the oleanane index. $\delta^{15}N_{org}$ vs the oleanane index. The C/N ratio vs 2-methylhopanes. The C/N ratio vs the ratio of C_{28} steranes/all steranes. The C/N ratio vs $\delta^{15}N$. The C/N ratio vs isorenieretane. $\delta^{15}N_{org}$ vs isorenieretane. All bio-marker data courtesy of Boudinot et al., (*in prep*).

VI. Conclusions:

The high-resolution (87 sample) bulk elemental and stable isotope record from the SH1 core demonstrates the occurrence of highly dynamic trends in nitrogen cycling that appear to have been influenced by both the input of terrestrial nitrogen and changes in marine nitrogen cycling under deoxygenated conditions. Previous records have only showed a single shift in $\delta^{15}N_{org}$ from more positive values pre-OAE2 to more negative values during and after OAE2. The two-phase negative shifts in my record and the magnitude of these shifts (-4.58 and -6.03) illustrates a higher degree of variability in the marine environment than has previously been reported in other locations. The trends in C/N and $\delta^{15}N_{org}$ can best be explained by the situation of the SH1 core location at the margin of the WIS, under strong influences of both terrestrial organic matter input and marine organic matter input. These results support the hypothesis that changes in nitrogen cycling in a nearshore environment of the WIS were more dynamic than open ocean sites, and were influenced by the combined effects of water column oxygenation and terrestrial input.

The larger magnitude of the negative $\delta^{15}N_{org}$ shift occurs as a result of this this terrestrial input; without the terrestrial input, the $\delta^{15}N_{org}$ values at the base of the record would likely be lower and the shift in $\delta^{15}N_{org}$ would be likely be similar to previously reported records. The addition of terrestrial matter raised the values of $\delta^{15}N_{org}$ and C/N by bringing in ^{15}N enriched nitrogen and higher C/N ratio organic matter from terrestrial plant debris. The presences of two large shifts in $\delta^{15}N_{org}$ demonstrates the more dynamic nature of this site as these two large positive peaks in $\delta^{15}N_{org}$ suggest at least two large influxes of terrestrial matter into the site. These influxes may have overprinted the negative signal produced by the marine nitrogen isotopic end-member during these elevated $\delta^{15}N_{org}$ value intervals. It is important to remember that this is a bulk record from a coastal shallow water setting whereas the other records are mostly from open ocean sites, meaning that previous records likely show less influence from terrestrial sources than SH1.

Post-OAE2 there is a decrease in the variability of the C/N ratio and the values remain more stable until the end of the record, supporting the idea that OAE2-like conditions require an increased supply of nutrients to fuel primary production. As stated above we should expect large variations in the C/N ratio if large influxes of terrestrial organic matter were still being added into the marine environment. This implies that in this location the increase in available nutrients were predominately supplied from terrestrial sources, as once the C/N ratio stabilizes post-OAE2, the records from all other sources stabilize (i.e. the system became less terrestrially influenced and more marine influenced). This is again corroborated by the oleanane index dropping to near 0 during the same time period.

Complementary biomarker data provides support for both the proposed influxes of terrestrial organic matter and the build-up of a depleted ammonium reservoir. Large increases in the oleanane index corresponds with large increases in the C/N ratio and $\delta^{15}N_{org}$, supporting the interpretation of a terrestrial organic matter control on bulk nitrogen signals. The ratio of C_{28} steranes/all steranes supports the build-up of ammonium, as we can see an increase in this ratio at the same time we see our lowest values for $\delta^{15}N_{org}$ and the C/N ratio.

This record might also serve as a cautionary tale for the future considering the current trends in climate change. With rising atmospheric pCO_2 and thus rising temperatures we can expect rises in both sea-level and continental hydrology in some areas and decreases in others. There will also likely be increased seasonality which will in turn introduce more terrestrial organic matter into the many coastal regions of our oceans, fueling the productivity of primary producers. However, the amount of terrestrial derived nutrients being delivered into the oceans may be substantially higher in the future than during the Cretaceous due to the excessive use of nitrogen and phosphorus rich fertilizers. This fact could serve to compound on the conditions seen during OAE2 and serve to bring about the onset of these conditions faster than what

happened in the past. This provides another reason to support the reduction of CO_2 emissions and inorganic fertilizer additions in the future.

Acknowledgements:

I'd like to thank the members of my committee for taking time out of their busy schedules to evaluate my research. I'd also like to express my sincere gratitude to the following individuals: to Katie Snell for the use of her laboratory and for sparking my interest on the subject of stable isotopic analysis; to Brett Davidheiser-Kroll for being an awesome lab manager, for his all his help in troubleshooting/teaching, and snacks; to Julio Sepúlveda for his endless patience, awesome mentoring, and endless support. Finally, an extra special thanks to Garrett Boudinot for his tireless work across all aspects of this project. Garrett's positive attitude, unyielding work ethic, and passion for teaching made this project possible.

Appendix 1

1.a. The effect of changing C/N ratios:

As OAE2 black shales have characteristically high C/N ratios, I tested the EA-IRMS response to varying C/N ratio standards. To do this, I artificially varied the C/N ratios of known standards by adding varying amounts of glucose. I prepared five samples of three known standards: Acetanillide #1, Pugel, and L-glutamic acid. One sample of each standard was left unaltered and weighed out to reflect the standards known C/N ratio. In the remaining four samples, glucose was added to raise the C/N ratios to 10, 30, 50, and 100 respectively.

After running three different standards at various C/N ratios, I found that $\delta^{15}N_{org}$ values remained relatively consistent across the run, with the exception of the samples with a C/N ratio of 100 (Fig. 12).

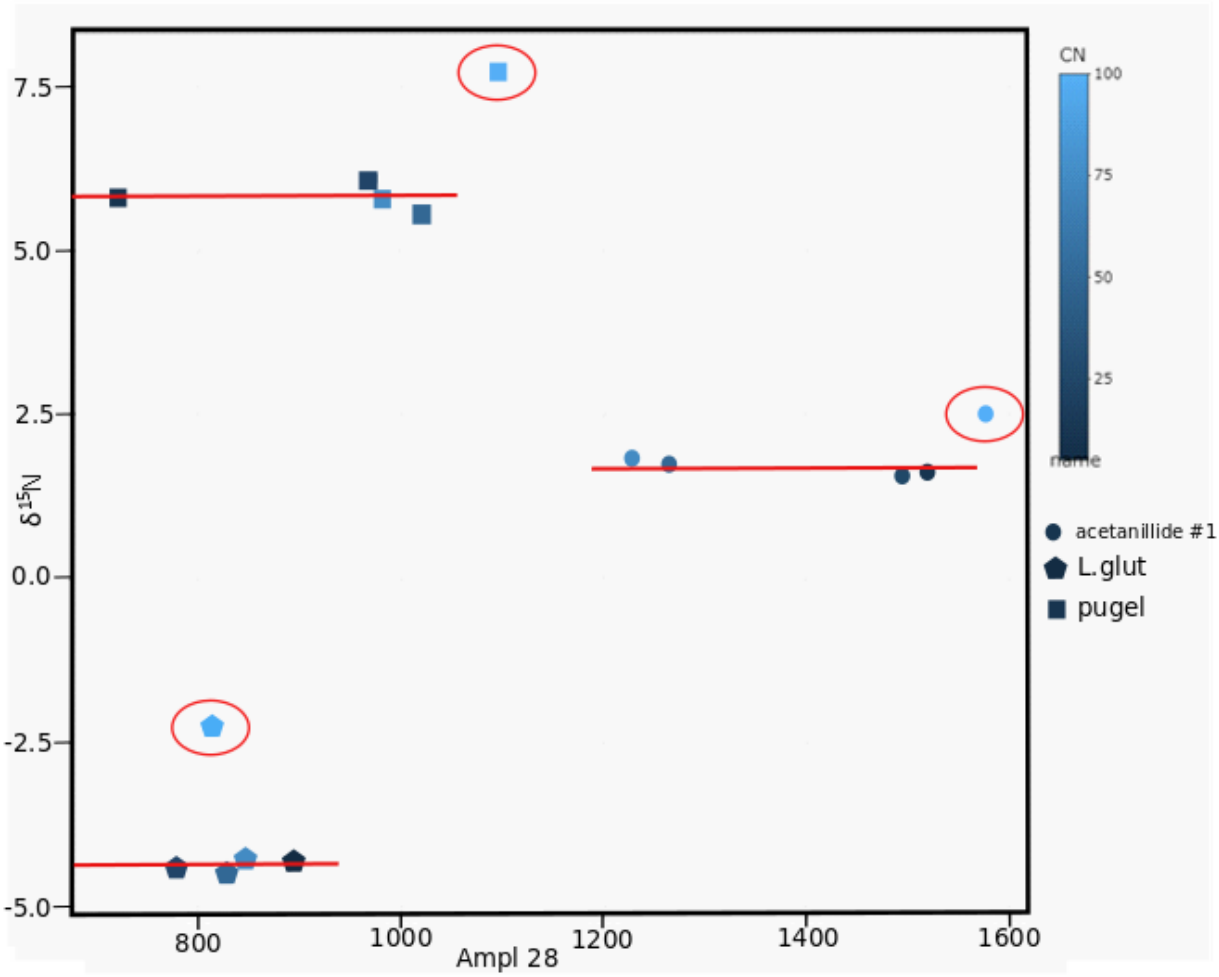

Figure 12**:** Standards plotted by $\delta^{15}N_{org}$ vs Amplitude28. Standards are identified by shape, with circles representing Acetanillide #1, pentagons representing L-glutamic acid, and squares representing Pugel. Lighter blue indicates a higher C/N ratio. Averages of the samples excluding C/N 100 samples are indicated by red lines. 100 C/N are highlighted by red circles. Actual values can be seen in Appendix 2.

On all three of the standards tested, the values for the 100 C/N ratio samples showed considerably higher $\delta^{15}N_{org}$ values than the samples with lower C/N ratios. Without the 100 C/N samples, the standard deviation of the remaining samples ranges from 0.08 - 0.2 and the average $\delta^{15}N_{org}$ values measured are very close to the actual values of the standards.

1.b. The need for tin in large size samples.

The higher $\delta^{15}N_{org}$ values of the 100 C/N were likely caused as a result of their larger size, which lead to incomplete combustion in the reactor column. I tested this by implementing larger tin sample cups (10 x 10 mm) instead of 3 x 8 mm, thus increasing the amount of tin by ~30 mg. The temperature in the reactor column is normally 900-1050 ºC, but the heat from the combustion of tin capsules raises this temperature to 1800 ºC (Carter and Barwick, 2011). I assumed this increase in heat would ensure complete combustion of large sample sizes. For this test, I also replaced the previously used standards with two matrix matched soil standards (B2153 - Known Organic Soil and B2152 - Low Organic Soil) that I expected to closely match the carbon% and nitrogen% of the SH1 samples. The samples were weighted out to reflect 50, 75, and 100 µg nitrogen, so the sample weights ranged from ~38 mg to ~88 mg. I also added extra tin (11.861 mg) to one sample and glucose (11.530 mg) to another. This was to determine if an excess of tin had any effect on our measurement and to confirm the results of the last test of C/N ratios. The results (Fig. 13) showed a fairly consistent measurement of $\delta^{15}N_{org}$. The standard deviation for B2152 was 0.2‰ and the standard deviation for B2153 was 0.07‰. This suggests that the increased heat generated by the higher amount of tin in the reactor column was effective at fully combusting the larger sample sizes, even with an excess of tin. It also confirmed the results of the first experiment that varying C/N ratios with glucose does not affect the measurement of $\delta^{15}N_{org}$ when sample is completely combusted.

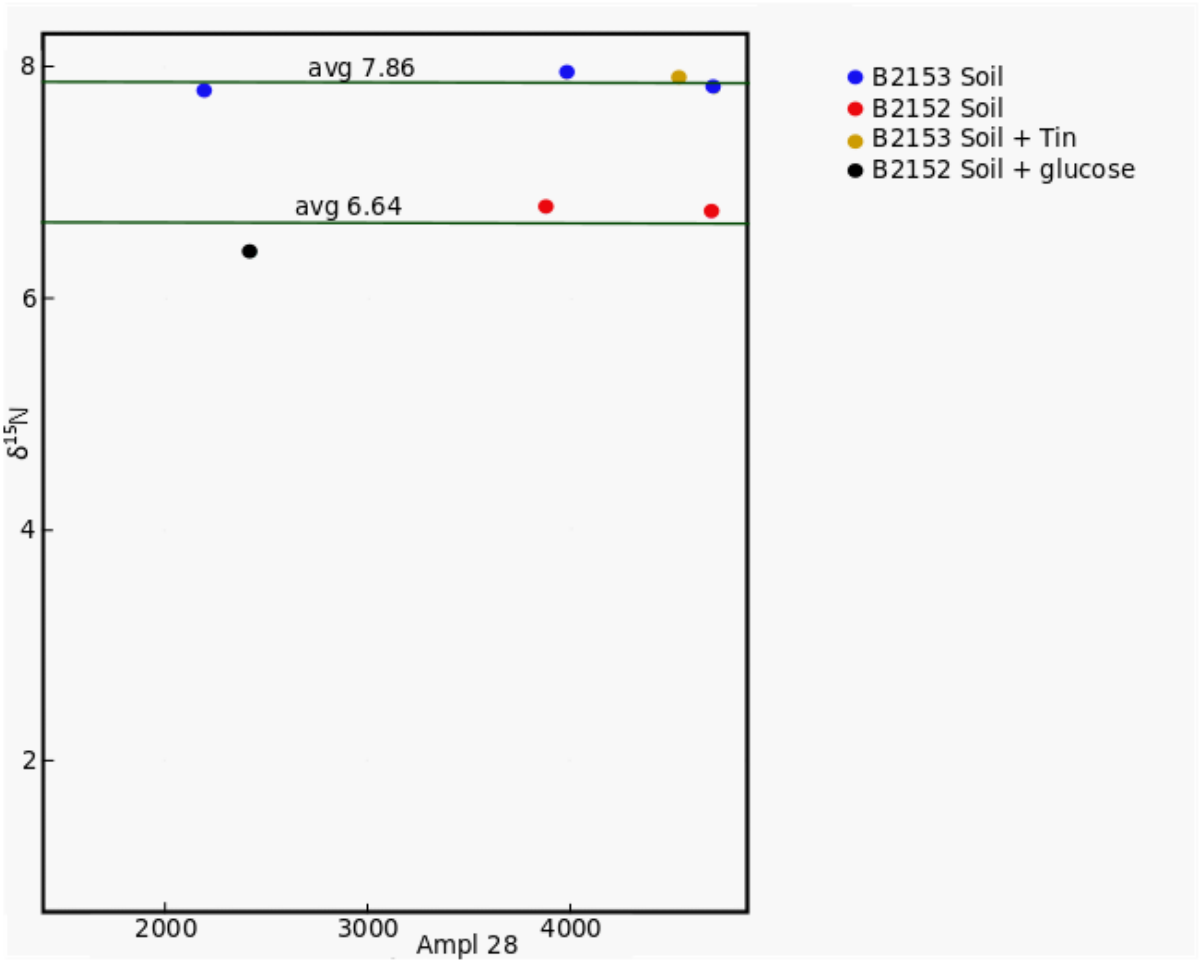

Figure 13: Samples plotted by $\delta^{15}N_{org}$ vs Amplitude28. Blue points are samples of B2153 Soil. Red points are samples B2152. Gold points indicate a sample of B2153 with extra Tin. Black points indicate a sample of B2152 with added glucose. The green lines show the average $\delta^{15}N_{org}$ of B2153 and B2152. Actual values can be seen in Appendix 2.

1.c. Silicate-rich samples

Carbon and nitrogen are bound to organics in a silicate matrix (black shales). I tested the removal of silicates to concentrate C and N using hydrofluoric acid (Knies, et al, 2007). The removal of silicates with HF is a costly, time consuming and potentially hazardous procedure. Using a silicate-rich soil standard, I demonstrated that pre-treatment with HF was not necessary for the purpose of measuring $\delta^{15}N_{org}$ and $\delta^{13}C_{org}$, and allowed for more rapid analyses of rock-bound organic matter without HF. Recent work by Brauer and Hahne (2005) supports these results. Brauer and Hahne (2005) showed that accurate measurement of sedimentary-bound $\delta^{15}N_{org}$ is possible on an EA-MS as long as complete combustion takes place. Complete

combustion of the silicate lattices liberates the ammonium of sediments allowing for accurate measurement of the total N contained within samples. The complete combustion of samples was achieved by adding larger tin sample cups thereby increasing the heat of the reactor column to 1800 C.

It should be noted that running silicate rich samples on an EA will lead to faster degradation of the reactor column. This effect can be mitigated by using a Ni insert in the reactor column. The Ni insert will slow the degradation of the column, but it will still be faster than running non-silicate materials.

1.d. Dealing with sample contaminates

When testing the analysis of pilot SH1 samples, the background mass 30 and mass 46 trace of the IRMS steadily increased with each run of an SH1 sample. The reference gas peaks also showed elevated baseline values which decreased over time when blanks or empties were run. I interpreted this as the presence of contaminants in the samples that may bleed over to later analyses. This 'bleed over' manifested as an elevated baseline for mass 46 (Fig. 14) and elevated N_2 reference gas peaks (Fig. 15). (Fig. 14) The top chromatograph shows a normal carbon peak with traces starting out near zero. The bottom chromatograph shows the elevated baseline for mass 46, seen in dark blue, starting off at over 100 mV in intensity. This elevated baseline made the accurate measurement impossible of carbon isotopes impossible as the area under the mass 46 peak is factored into calculating δ13Corg.

We see the elevated readings of the reference gas and subsequent reference gas peaks decreasing with time (Fig. 15). These peaks and gas traces should be flat and consistent with time, and the difference between the two reference peaks should be within 0.02. The fact that they are not demonstrates the presence of an unknown contaminate slowing be purged from the system by the normal flow of He through the system.

To solve this, I added empty Tin capsules (blanks) after each sample of SH1. These blanks allowed time for the normal flow of He gas through the EA to purge any contaminants being produced by the combustion of samples. This problem also demonstrated the need for a shorter number of samples per run as measurements seemed to degrade the longer the runs lasted.

While this did help it did not fully solve the problem. It was proposed that degradation of the reactor column may have been responsible for this issue, but the issue was still present when brand new columns were used. We still cannot fully explain the cause of these issues. Further investigation is needed to fully correct this issue.

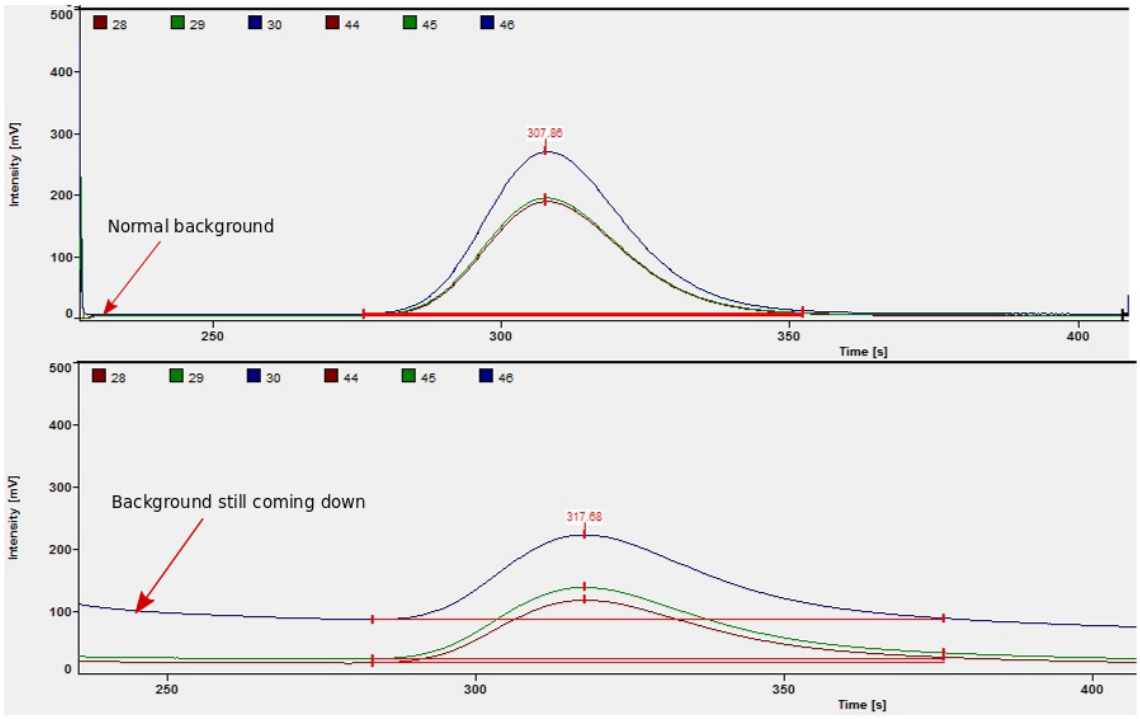

Figure 14: Chromatograph of two carbon peaks. The top chromatograph shows a normal background trace. The bottom shows an elevated background trace that is still decreasing prior to the sample peak.

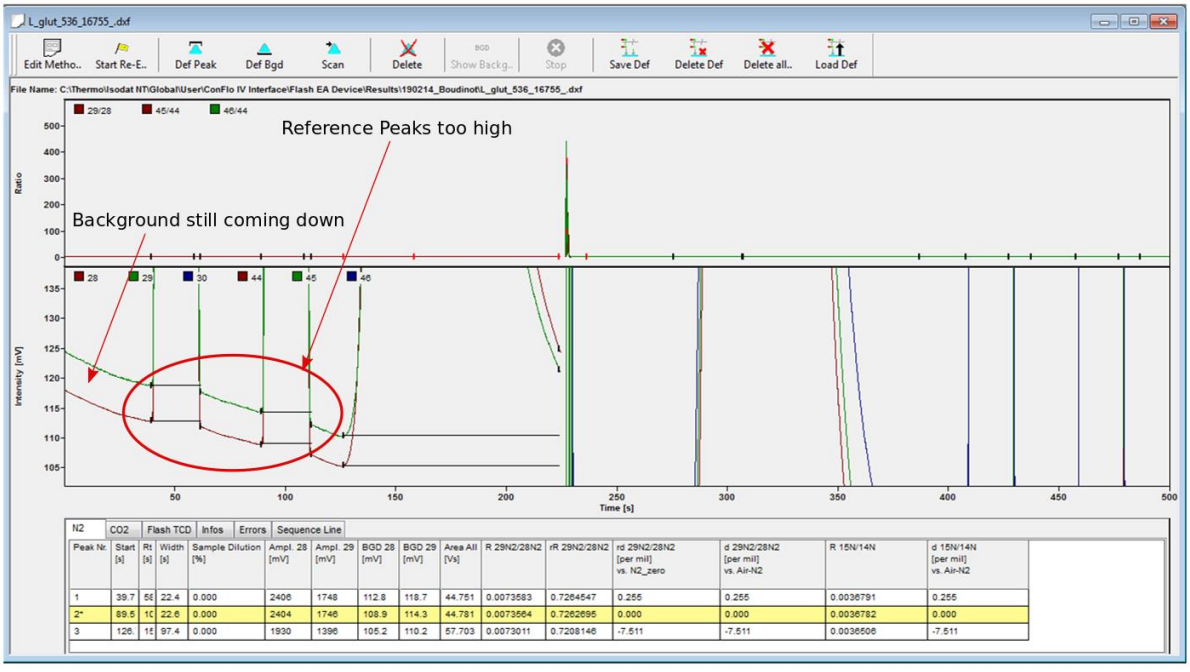

Figure 15: Chromatograph showing elevated reference peaks and elevated background still in the process of decreases at the start of a run.

References:

D. D. Adams, M. T. Hurtgen, and B. B. Sageman, 2010, Volcanic triggering of a biogeochemical cascade during Ocean Anoxic Event 2: Nature Geoscience, v. 3, pp. 201-204.

R.S. Barclay, J.C. McElwain, and B.B. Sageman, 2010, Carbon sequestration activated by a volcanic CO2 pulse during Ocean Anoxic Event 2: Nature geoscience, v. 3, pp. 205-208.

Ruvalcaba Baroni, I., N. A. G. M. van Helmond, I. Tsandev, J. J. Middelburg, and C. P. Slomp (2015), The nitrogen isotope composition of sediments from the proto-North Atlantic during Oceanic Anoxic Event 2, *Paleoceanography*, *30*, 923–937, doi:10.1002/2014PA002744.

Behrooz, L., Naafs, B. D. A., Dickson, A. J., Love, G. D., Batenburg, S. J., & Pancost, R. D. (2018). Astronomically driven variations in depositional environments in the South Atlantic during the Early Cretaceous. Paleoceanography and Paleoclimatology, 33, 894–912. https:// doi.org/10.1029/2018PA003338

Blakey, R. C., & Ranney, W. (2018). *Ancient landscapes of western North America: A geologic history with paleogeographic maps*. Cham, Switzerland: Springer. ISBN-13: 978-3319596341

Bräuer, K., & Hahne, K. (2005). Methodical aspects of the 15N-analysis of Precambrian and Palaeozoic sediments rich in organic matter. *Chemical Geology*, *218*(3-4), 361-368.

Brodie, C. R., Casford, J. S., Lloyd, J. M., Leng, M. J., Heaton, T. H., Kendrick, C. P., & Yongqiang, Z. (2011). Evidence for bias in C/N, $\delta^{13}C_{org}$ and $\delta^{15}N_{org}$ values of bulk organic matter, and on environmental interpretation, from a lake sedimentary sequence by pre-analysis acid treatment methods. *Quaternary Science Reviews*, *30*(21-22), 3076-3087.

J.F. Carter and V.J. Barwick (Eds), Good Practice guide for isotope ratio mass spectrometry, FIRMS (2011). ISBN 978-0-948926-31-0

C. Deutsch, Sarmiento, J.L., Sigman, D.M., Gruber, N., and Dunne, J.P., 2007, Spatial coupling of nitrogen inputs and losses in the ocean: nature, v. 445, pp. 163-167.

A.D.C., DuVivier, D. Selby, B.B. Sageman, I. Jarvis, D.R. Grocke, and Silke Voigt, 2014, Marine 187Os/188Os isotope stratigraphy reveals the interaction of volcanism and ocean circulation during Oceanic Anoxic Event 2: Earth and Planetary Science Letters, v. 389, pp. 23-33.

A.D.C., DuVivier, A.D. Jacobson, G.O., Lehn, D. Selby, M.T. Hurgen, and B.B. Sageman, 2015, Ca isotope stratigraphy across the Cenomanian-Turonian OAE2: Links between volcanism, seawater geochemistry, and the carbonate fractionation factor, Earth and Planetary Science Letters v. 416, pp. 121-131.

S. Flogel, K. Wallmann, C.J. Poulden, J. Zhou, A. Oschlies, S. Voigt, and W. Kuhnt, 2011, Simulating the biogeochemical effects of volcanic CO2 degassing on the oxygen-state of the deep ocean during the Cenoanian/Turonian Anoxic Event (OAE2): Earth and Planetary Science Letters, v. 305, I. 3-4, pp. 371-384.

Oliver Friedrich, Richard D. Norris, Jochen Erbacher; Evolution of middle to Late Cretaceous oceans—A 55 m.y. record of Earth's temperature and carbon cycle. *Geology* ; 40 (2): 107–110. doi: https://doi.org/10.1130/G32701.1

N. Gruber, and J.L. Sarimento, 1997, Global patterns of marine nitrogen fixation and denitrification: Global Biogeochemical Cycles, v.11, no. 2, pp. 235-266.

J.D. Hays and W.C. Pitman, 1973, Lithospheric plate motion, sea level changes, and climatic and ecological consequences: Nature, v. 246, pp. 18-22.

M. B. Higgins, R. S. Robinson, J. M. Husson, S. J. Carter, A. Pearson, 2012, Dominant eukaryotic export production during ocean anoxic events reflects the importance of recycled NH4+: Proceedings of the National Academy of Science, v. 109 no. 7, pp. 2269-2274.

S. K. Hong and Y. I. Lee, 2012, Evaluation of atmospheric carbon dioxide concentrations during the Cretaceous: Earth and Planetary Science Letters, v. 327-328, pp. 23-28.

Jones, M. M., Sageman, B. B., Oakes, R. L., Parker, A. L., Leckie, R. M., Bralower, T. J., ... & Fortiz, V. (2019). Astronomical pacing of relative sea level during Oceanic Anoxic Event 2: Preliminary studies of the expanded SH# 1 Core, Utah, USA. *Geological Society of America Bulletin*.

C.K. Junium and M.A. Arthur, 2007, Nitrogen cycling during the Cretaceous, Cenomanian-Turonian Oceanic Anoxic Event II: Geochemistry, Geophysics, Geosystems, v. 8, no. 3, pp. 1-18.

Y. Kashiyama, N.O. Ogawa, J. Kuroda, M. Shiro, S. Nomoto, R. Tada, H. Kitazato, and N. Ohkouchi, 2008, Diazotrophic cyanobacteria as the major photoautotrophs during mid-Cretaceous oceanic anoxic events: Nitrogen and carbon isotopic evidence from sedimentary porphyrin: Organic Geochemistry, v. 39, pp. 532-549.

A.C. Kerr, 2005, Oceanic LIPs: the kiss of death: Elements, v. 1, no. 5, pp. 289-292

Knies, J., Brookes, S., & Schubert, C. J. (2007). Re-assessing the nitrogen signal in continental margin sediments: New insights from the high northern latitudes. Earth and Planetary Science Letters, 253(3-4), 471-484. doi:10.1016/j.epsl.2006.11.008

M.A. Kominz, 1984, Oceanic ridge volumes and sea-level change – an error analysis: In: Schlee, J.S., Ed., Interregional Unconformities and Hydrocarbon Accumulation, 36, American Association of Petroleum Geologists, Tulsa, pp. 109-127.

Kuhnt, W., Holbourn, A. E., Beil, S., Aquit, M., Krawczyk, T., Flögel, S., Chellai, E. H., and Jabour, H. (2017),Unraveling the onset of Cretaceous Oceanic Anoxic Event 2 in an extended sediment archive from the Tarfaya-Laayoune Basin, Morocco, *Paleoceanography*, 32, 923– 946, doi:10.1002/2017PA003146.

M.M.M. Kuypers, R.D. Pancost, I.A. Nijenhuis, and J.S. Sinninghe Damste, 2002, Enhanced productivity led to increased organic carbon burial in the euxinic North Atlantic basin during the late Cenomanian oceanic anoxic event: Paleoceanography, v. 14, no. 4, pp. 1-13.

M. M. M. Kuypers, Y. van Breugel, S. Schouten, E. Erba, and J. S. Sinninghe Damste, 2004, N2-fixing cyanobacteria supplied nutrient N for Cretaceous ocean anoxic events: Geology, v. 32, no. 10, pp. 853-856.

R.L. Larson, 1991, Latest pulse of Earth: Evidence for a mid-Cretaceous superplume: Geology, v. 19, pp. 547-550.

K.M. Meyer and L.R. Kump, 2008, Oceanic Euxinia in Earth History: Causes and Consequences: Annual Review of Earth and Planetary Sciences, v. 36, pp. 251-288.

C.L. O'Brien, S.A. Robinson, R.D. Pancost, J.S. Sinninghe Damste, S. Schouten, D.J. Lunt, H. Alsenz, A. Bornemann, C. Bottini, S.C. Brassell, A. Farsworth, A. Forster, B.T. Huber, G.N. Inglis, H.C. Jenkyns, C. Linnert, K. Littler, P. Markwick, A. McAnena, J. Mutterlose, B.D.A Naafs, W. Puttmann, A. Slujis, N.A.G.M. van Helmond, J. Vellekoop, T. Wagner, and N.E. Wrobel, 2017, Cretaceous sea-surface temperature evolution: Constraints from TEX86 and planktonic foraminiferal oxygen isotopes: Earth-Science Reviews, v. 172, pp. 224-247.

N. Ohkouchi, Y. Kashiyama, J. Kuroda, N. O. Ogawa, and H. Kitazato, 2006, The importance of diazotrophic cyanobacteria as primary producers during Cretaceous Ocean Anoxic Event 2: Biogeosciences v. 3, pp. 467-478.

IPCC, 2014: Climate Change 2014: Synthesis Report. Contribution of Working Groups I, II and III to the Fifth Assessment Report of the Intergovernmental Panel on Climate Change [Core Writing Team, R.K. Pachauri and L.A. Meyer (eds.)]. IPCC, Geneva, Switzerland, 151 pp.

K.E. Peters, C.C. Walters, and J.M. Moldowan (2005). The biomarker guide, Cambridge University Press, p. 1155.

Petersen, S. V., Tabor, C. R., Lohmann, K. C., Poulsen, C. J., Meyer, K. W., Carpenter, S. J., ... & Sheldon, N. D. (2016). Temperature and salinity of the Late Cretaceous western interior seaway. *Geology*, *44*(11), 903-906.

Popp, B., Isocamp Lecture 2016, courtesy of Boudinot, F.G.

Prauss, M.L., 2007, Availability of reduced nitrogen chemospecies in photic-zone waters as the ultimate cause for fossil prasinophyte prosperity: Palaios, v. 22, pp. 489-499.

G.H. Rau, M.A. Arthur, and W.E. Dean, 1987, 15N/14N variations in Cretaceous Atlantic sedimentary sequences: Implications for past changes in marine nitrogen biogeochemistry: Earth and Planetary Science Letters, v. 82, pp. 269-279.

Sinninghe Damsté, J. S., & Schouten, S. (2006). Biological markers for anoxia in the photic zone of the water column. In *Marine organic matter: Biomarkers, isotopes and DNA* (pp. 127-163). Springer, Berlin, Heidelberg.

Takashima, R., Nishi, H., Huber, B. T., & Leckie, R. M. (2006). Greenhouse world and the Mesozoic ocean. *Oceanography*, v. 19, no. 4, 64-74.

X. Zhang, D.M. Sigman, F.M.M. Morel, and A.M.L. Kraepiel, 2014, Nitrogen isotope fractionation by alternative nitrogenases and past ocean anoxia: Proceedings of the National Academy of Sciences, v. 111, no. 13, pp. 4782-4787.